Article

Antimicrobial Peptide−Poly(ethylene glycol) Conjugates: Connecting Molecular Architecture, Solution Properties, and Functional Performance

Zixian Cui, Matthew A. Crawford, Blake A. Rumble, Megan M. Krogh, Molly A. Hughes, and Rachel A. Letteri*

Read Online

ACCESS | 📊 Metrics & More | 📖 Article Recommendations | 🆂🆘 Supporting Information

ABSTRACT: Antimicrobial peptides (AMPs) are promising alternatives to conventional antibiotics for treating infections caused by drug-resistant bacteria; yet, many peptides are limited by toxicity to eukaryotic cells and instability in biological environments. Conjugation to linear polymers that reduce cytotoxicity and improve stability, however, often decreases antimicrobial activity. In this work, we combine the biocompatibility advantages of poly(ethylene glycol) (PEG) with the efficacy merits of nonlinear polymer architectures that accommodate multiple AMPs per molecule. By conjugating a chemokine-derived AMP, stapled Ac-P9, to linear and star-shaped PEG with various arm numbers and lengths, we investigated the role of molecular architecture in solution properties (i.e., ζ-potential, size, and morphology) and performance (i.e., antimicrobial activity, hemolysis, and protease resistance). Linear, 4-arm, and 8-arm conjugates with 2−2.5 kDa PEG arms were found to form nanoscale structures in solution with lower ζ-potentials relative to the unconjugated AMP, suggesting that the polymer partially shields the cationic AMP. Reducing the length of the PEG arms of the 8-arm conjugate to 1.25 kDa appeared to better reveal the peptide, seen by the increased ζ-potential, and promote assembly into particles with a larger size and defined spherical morphology. The antimicrobial effects exerted by the short 8-arm conjugate rivaled that of the unconjugated peptide, and the AMP constituents of the short 8-arm conjugate were protected from proteolytic degradation. All other conjugates examined also imparted a degree of protease resistance, but exhibited some reduced level of antimicrobial activity as compared to the AMP alone. None of the conjugates caused significant cytotoxic effects, which bodes well for their future potential to treat infections. While enhancing proteolytic stability often comes with the cost of lower antimicrobial activity, we have found that presenting AMPs at high density on a neutral nonlinear polymer strikes a favorable balance, exhibiting both enhanced stability and high antimicrobial activity.

KEYWORDS: star-shaped, antimicrobial peptide, poly(ethylene glycol), peptide−polymer conjugates, self-assembly
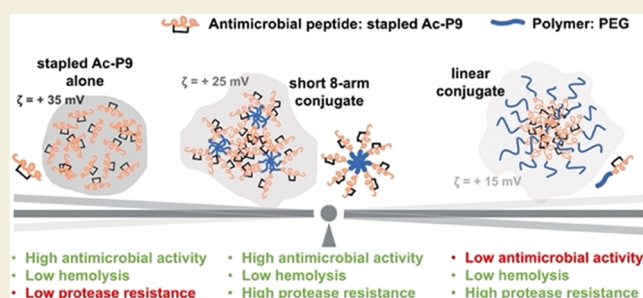
■ INTRODUCTION

The use of antibiotics leads bacteria to develop resistance. Antimicrobial-resistant bacteria are a mounting problem that are predicted to cause infections that will result in 10 million deaths globally each year and cost trillions of dollars annually by 2050.[1,2] Therefore, novel antimicrobial agents are critically needed to treat life-threatening infections and lower the associated healthcare costs. As one promising class of therapeutic candidates, cationic antimicrobial peptides (AMPs) can kill bacteria, in many cases by inducing membrane disruption via hydrophobic and electrostatic interactions with bacterial membranes. These peptides are often helical, can kill antibiotic-resistant organisms, and invoke the development of resistance more slowly, and to a lesser degree, than conventional antibiotics.[3,4] However, the clinical implementation of many AMPs remains limited by rapid clearance,

susceptibility to proteases, and toxicity to mammalian cells, among other factors.[5] According to a 2022 report on the Data Repository of Antimicrobial Peptides (DRAMP), only 0.4% of over 20,000 known AMPs have entered preclinical or clinical trials and only 12 are on the market.[6,7]

Toward overcoming the aforementioned translational challenges, AMPs can be modified at the molecular level (e.g., changing chirality, substitution with unnatural amino, and/or cyclization)[8,9] and/or delivered in carriers spanning a

range of inorganic (e.g., gold-, silver-, and silica-based nanoparticles) and organic (e.g., polymer, micelle, liposome, and hydrogel) compositions.[10] In general, carriers typically improve the solubility of AMPs, reduce cytotoxicity, slow proteolytic degradation, and yield larger, but still stealthy, molecules that evade rapid renal or immune-mediated clearance.[11] Among the variety of modifications, attaching AMPs to synthetic polymers is particularly attractive since it allows control of composition and architecture over a vast design space, providing opportunities to tailor conjugates toward meeting the complex demands of realizing *in vivo* efficacy for a given application or route of administration.[12−14]

The simplest design of AMP−polymer conjugates involves appending AMPs to the end of a long linear polymer chain. Although conjugating AMPs to one end of neutral hydrophilic polymers, for example, poly(ethylene glycol) (PEG), shields the AMP from proteolytic degradation and toxic interactions with eukaryotic cells, the PEG chain can also preclude the AMP from intended interactions with bacterial membranes, thereby markedly reducing antimicrobial activity.[15,16] Short-ening the PEG chain can restore high antimicrobial activity[17,18] but sometimes at the expense of desirable qualities, such as protease resistance and/or compatibility with mammalian cells.[19]

Advances in polymer chemistry allow the preparation of AMP−polymer conjugates with a variety of architectures (e.g., star-shaped, comb-like, and hyperbranched) that accommodate multiple AMPs on a single molecule. Compared to unconjugated peptides and/or linear conjugates, these non-linear architectures provide opportunities to better balance antimicrobial activity, biocompatibility, and protease resistance.[13,20−22] For example, conjugates having multiple poly-(lysine-*co*-valine) AMP arms attached to a poly(amido amine) core exhibit superior antibacterial activity relative to the poly(lysine-*co*-valine) AMP alone.[20,23] Increasing the number of AMP arms from 4 to 16 on these star-shaped conjugates further enhances activity, presumably due to the higher local concentration of the AMPs.[23,24] Besides the increase in antimicrobial activity, star-shaped poly(lysine)-polyethyleni-mine conjugates better resist proteolytic degradation than linear poly(lysine) AMP alone with a similar total number of lysine units.[24] Notably, on star-shaped conjugates with neutral glucosamine polymer arms, increasing the fraction of cationic peptide arms enhanced activity against methicillin-resistant *Staphylococcus aureus* (MRSA) without compromising compat-ibility with red blood cells and human aortic smooth muscle cells.[25]

Despite encouraging findings with the star-shaped AMP-glucosamine conjugates,[25] few other studies on nonlinear AMP−polymer conjugates involve neutral hydrophilic poly-mers, potentially due to concerns that supramolecular assembly in solution may hide the hydrophobic AMP in ways that reduce antimicrobial activity. Yet, several linear AMP-PEG conjugates that assemble into micelles or nanoparticles with peptide cores and PEG shells exhibit antimicrobial activity comparable to the unconjugated peptide, a result attributed to the high local concentration of AMPs.[26,27] Moreover, compared to the peptide alone, these supramolecular structures exhibit lower toxicity to mammalian cells presum-ably due to the shielding effects of PEG. Similar to linear conjugates, the literature on star-shaped amphiphilic block copolymers[28] suggests that nonlinear conjugates may form supramolecular assemblies as well, either with AMP cores

surrounded by PEG shells, or vice versa, in aqueous solution. Thus, to fully leverage the therapeutic promise of nonlinear conjugates between AMPs and neutral hydrophilic polymers, it will be important to understand their assembly in solution and how it connects to functional performance, a topic that remains largely unexplored.

Accordingly, in this work, we prepared a series of linear and star-shaped AMP−PEG conjugates with varying arm number and length to investigate the effects of molecular architecture on solution assembly and antimicrobial performance. We chose to compare linear and star-shaped conjugates due to the commercial availability of linear and star-shaped maleimide-functionalized PEG that allows us to conjugate thiol-terminated AMPs. Keeping AMP equivalent concentrations constant, we measured particle size, morphology, and ζ-potential to understand how the conjugates assemble in solution and present AMPs. We then evaluated antimicrobial activity, hemolysis, and proteolytic stability at the same peptide equivalent concentrations as those used for studying conjugate assembly in solution. We anticipate that the characterizations and findings reported in this work can be extended to other helical AMP−polymer conjugates to build structure−prop-erty−performance relationships and further expand the design space to accelerate the application of AMPs.

■ MATERIALS AND METHODS

Materials

Fmoc-L-Cys(Trt)-OH (≥98%), Fmoc-L-Gly-OH (≥98%), Fmoc-L-Pro-OH (≥98%), Fmoc-L-Glu(OtBu)-OH (≥98%), Fmoc-L-Ser-(Trt)-OH (≥98%), Fmoc-L-Lys(Boc)-OH (≥98%), Fmoc-L-Leu-OH (≥98%), Fmoc-L-Val-OH (≥98%), Fmoc-(S)-2-(4-pentenyl)-Alanine-OH (≥97%), rink amide resin LS (0.5 mmol/g, 100−200 mesh), and oxyma pure (≥99%) were purchased from Advanced ChemTech. N,N-dimethylformamide (DMF, ≥99.8%), acetic anhy-dride (≥98%), piperidine (≥99%), diisopropyl carbodiimide (DIC, ≥99%), Grubbs Catalyst Generation I (M102, ≥97%), 1,2-dichloro-ethane (DCE) (≥99%), dichloromethane (DCM, ≥ 99.5%), diethyl ether (≥99%), 2,2′-(ethylenedioxy)diethanethiol (DODT, ≥95%), triisopropylsilane (TIPS, ≥98%), trifluoroacetic acid (TFA, ≥99%), acetonitrile (ACN, for HPLC, gradient grade, ≥99.9%), methoxy-PEG-maleimide (linear PEG maleimide, average M_n = 2 kDa), 4-arm PEG-maleimide (average M_n = 10 kDa), 8-arm PEG-maleimide (average M_n = 20 kDa), 8-arm PEG-maleimide (average M_n = 10 kDa), deuterium oxide (D$_2$O), phosphate-buffered saline (PBS), 2,2,2-trifluoroethanol (TFE, ≥99%), sodium trifluoroacetate (NaT-FAc, ≥98%), DL-dithiothreitol (DTT, ≥98%), potassium phosphate monobasic (≥99%), potassium phosphate dibasic (≥98%), sodium dodecyl sulfate (SDS, ≥99%), Proteinase K from *Tritirachium album*, lysogeny broth (LB)-Lennox, sodium chloride (≥99%), RPMI 1640 medium with or without phenol red, low-endotoxin bovine serum albumin (BSA), Triton X-100, and melittin were purchased from Sigma-Aldrich. The cell viability reagent alamarBlue was purchased from ThermoFisher.

Instrumentation

Reverse-phase analytical high-performance liquid chromatography (HPLC) was performed at 35 °C with a flow rate of 1 mL/min on an Alliance system from Waters equipped with an XBridge C18 column (4.6 × 50 mm^2, 3 μm) and a photodiode array detector (Waters 2489 UV/Visible) to assess the purity of peptides and conjugates, as well as to monitor the progress of conjugation reactions and dialysis. Preparative HPLC, using a C18 column (30 mm × 150 mm, 5 μm) at room temperature with a flow rate of 25.52 mL/min and a photodiode array detector (Waters 2489 UV/Visible), was used to purify crude peptides and conjugates. Samples were prepared in HPLC solvent (5% v/v ACN/water with 0.1% TFA).

NMR spectroscopy was conducted on an 800 MHz Burke Avance III Varian NMR spectrometer in D_2O. Chemical shifts were referenced to the solvent residual peak at 4.79 ppm. Spectra were analyzed with MestReNova v14.3.2-32681.

Matrix-assisted laser desorption/ionization-time-of-flight (MALDI-TOF) mass spectrometry (MS) was performed on a Shimadzu MALDI-8030 system with a 200 Hz solid-state laser (355 nm). The instrument was calibrated with a standard MALDI calibration kit (TOFMix by Shimadzu, 670 fm/μL in 70% v/v ACN with 0.1% TFA). Samples (1 μL, 2 mg/mL in HPLC solvent) were coated with a α-cyano-4-hydroxycinnamic acid (CHCA) matrix (1 μL, 5 mg/mL in 70% v/v ACN with 0.1% TFA) on a stainless-steel plate and thoroughly dried in air before measurement.

Size exclusion chromatography (SEC) was performed in TFE with 0.02 M NaTFAc at a rate of 0.3 mL/min using a Tosoh system equipped with two isocratic pumps (one for the sample, the second for the solvent reference), a degasser, an autosampler, one 4.6 mm × 35 mm TSKgel guard super AW-H column (bead diameter: 9 μm), two 6 mm × 150 mm TSKgel super AWM-H linear analytical columns (beads diameter: 9 μm), and a refractive index detector. Number-average molecular weight (M_n) and dispersity ($Đ$) were determined relative to those of poly(methyl methacrylate) (PMMA) standards. Samples were prepared at concentrations of 2−3 mg/mL with an injection volume of 20 μL.

Dynamic light scattering (DLS) and ζ-potential measurements were performed on a Malvern Zetasizer Ultra with 4.0 mW laser (633 nm) at 25 °C. Samples were prepared at concentrations of 100, 200, and 400 μM peptide in 10 mM PBS (pH = 7.4) and filtered (0.45 μm, PTFE) before measurement. Size measurements were performed in square DTS0012 cuvettes (Malvern) in triplicate. To validate the DLS results determined using the manufacturer's software (ZS Xplorer 2.10), we fitted the correlograms using a nonlinear cumulant analysis with decay models, including either one or multiple size distributions of the particles.[29] We found that the results fitted from the single population model were consistent with the Z-average diameters reported from DLS, and the results from the bimodal distribution were close to the two peaks on the intensity profile generated from DLS software. We suspect that the two populations correspond to single chains (unimers) and assemblies. The diameters of the assemblies from the bimodal fitting were larger than the Z-average diameters. Considering that larger structures contribute more than smaller particles to intensity-averaged DLS Z-average sizes, we used the Z-average diameters as the hydrodynamic diameters of the particles. We found that the mass concentration of the unconjugated peptide at 200 μM was only 0.6 mg/mL, which led to weak scattering and low data quality when using DLS; thus, the hydrodynamic diameter of the unconjugated peptide could not be determined. The diffusion barrier technique described by the manufacturer was used for ζ-potential measurements to protect the peptide-based material and the electrodes in DTS1070 cuvettes.[30] Buffer (0.8 mL) was preloaded in the cuvette, and sample solution (50 μL) was slowly added to the bottom of the cuvette using a gel-loading pipet tip to minimize convective mixing. ζ measurements were performed in triplicate and reported as the mean ± the standard deviation. Both size and ζ-potential were measured in 10 mM PBS to limit the salt concentration and permit calculation of ζ-potential from electrostatic mobility using the Smoluchowski approximation.[31]

Transmission electron microscopy (TEM) was performed using an FEI Titan instrument operating at an accelerating voltage of 120 kV. Peptide and conjugate samples were prepared at peptide equivalent concentrations of 200 μM in 10 mM PBS (pH = 7.4). Carbon-coated copper grids (300 mesh, Electron Microscopy Sciences) were pretreated with 20% v/v $O_{2(g)}$ and 80% v/v $Ar_{(g)}$ in a plasma cleaner for 30 s. Samples (3 μL) were added to the grids for 1 min, blotted with filter paper by placing filter paper at the edge of the grid to remove excess solution, and washed three times by quickly dabbing and blotting off a drop of deionized (DI) water (10 μL). Washed grids were dried for 1 min before being stained with 2% aqueous uranyl acetate solution (3 μL) for 1 min. Excess uranyl acetate solution was blotted off with filter paper and the samples were air-dried before imaging at magnifications ranging from 43,000 to 87,000×. Particle diameters were measured using ImageJ. Histograms were generated in Excel from counts of 200 structures per sample.

Peptide Synthesis, Deprotection, and Purification

Prestapled Ac-P9:Ac-PESKAIKA(pentenyl)LLKA(pentenyl)-VSKERSKRSP-NH$_2$ and prestapled Ac-CGGP9 used for conjugation to PEG maleimide:Ac-CGGPESKAIKA(pentenyl)LLKA(pentenyl)-VSKERSKRSP-NH$_2$ were synthesized using a CEM Liberty Blue microwave-assisted solid-phase peptide synthesizer via standard Fmoc methods on a rink amide resin (0.5 mmol/g, Advanced ChemTech). Fmoc-protecting groups on the resin and amino acids were removed using 20% (v/v) piperidine in DMF at 90 °C for 70 s. For the coupling of amino acids (0.2 M in DMF), diisopropyl carbodiimide (DIC, 1 M in DMF) and Oxyma Pure (1 M in DMF) were added at 90 °C for 4 min. Acetyl capping of the N-terminal amine was achieved by the reaction with acetic anhydride (10% v/v in DMF) at 65 °C for 2 min 30 s. All arginine residues were coupled twice prior to Fmoc deprotection in an effort to prevent deletions.

Stapling was conducted via a ring-closing metathesis reaction on resin between the alkene groups of the pentenyl alanine residues in a 10 mM solution of Grubbs first-generation catalyst in DCE. Peptide-loaded resin was washed with DCE to remove DMF before the addition of the catalyst solution. The catalyst solution was deoxygenated with bubbling $N_{2(g)}$ at room temperature for 20 min and then added to the resin-bound peptide in a reaction vessel to react for 30 min at 40 °C. The mixture was drained, and the peptide-bound resin was washed with DCE and then recharged with Grubbs catalyst solution under the same conditions as above. The mixture was drained and washed with DCE after the reaction.

An acidic cleavage cocktail of 92.5% (v/v) TFA, 2.5% (v/v) TIPS, 2.5% (v/v) DODT, and 2.5% (v/v) DI water was used to cleave the peptides from the resin and remove the side-chain protecting groups. After the peptide-bound resin was stirred with the deprotection cocktail for 3 h at room temperature, the mixture was filtered through a glass peptide synthesis vessel (25 mL). The peptide solution (20 mL) was collected and precipitated into cold diethyl ether in four centrifuge tubes (40 mL in each), isolated by centrifugation (4700 rpm, 5 min), washed twice with ether, and dried under vacuum. The peptides were stored at −20 °C before use. The yield of the crude peptide isolated after precipitation and vacuum drying was 85−90% for 0.25 mmol scale synthesis reactions.

Peptides were purified by preparative HPLC before characterization/conjugation. Crude peptides (30 mg) were dissolved in HPLC solvent (10 mL) and filtered through 0.45 μm PTFE syringe filters. The solution was injected and run, and then the product was collected and lyophilized. The elution profiles used on the preparative HPLC were calculated by scaling up the column size, injection volume, flow rate, and loading mass from the corresponding analytical HPLC method as recommended by Waters.[32] The recovery following purification was calculated as the mass ratio of purified peptide to injected crude peptide and therefore reflects both the purity of the crude peptide and the recovery from the chromatography system. The purity was determined by the % peak area on analytical HPLC, assuming similar extinction coefficients for the desired peptide and potential impurities. For each run, the recovery was ca. 30−40% from 30 mg of crude peptide, with purity >99%. Synthesis and purification were confirmed by MALDI-TOF MS. Stapled Ac−P9 m/z: [M + Na]$^+$ calculated = 2573.6; found = 2573.0 (Figure S1). Stapled Ac-CGGP9 m/z: [M + Na]$^+$ calculated = 2788.6; found = 2789.3 (Figure S2).

Conjugation of Stapled Ac-CGGP9 to Linear and Star-Shaped PEG Maleimide

Purified stapled Ac-CGGP9 was conjugated to linear, 4-, 8-, and short 8-arm PEG maleimide in 1× PBS (pH = 7.4). We conducted the conjugation reactions at pH 7.4 because while a lower pH may hinder the dimerization of the thiol-functionalized peptides, it is also possible that decreasing the reducing pH would decrease the reaction rate of the conjugation reaction and result in fewer peptide arms on the

prepared conjugates. For preparing the linear conjugate, PEG maleimide (24 mg, 12 μmol) and peptide (with 7 TFA counterions; 47 mg, 13.2 μmol) were dissolved in PBS (2.4 mL). For the 4-arm star-shaped conjugate, 4-arm PEG maleimide (28 mg, 2.8 μmol) and stapled Ac-CGGP9 (with 7 TFA counterions; 50 mg, 14 μmol, 5 equiv relative to 4-arm PEG) were dissolved in PBS (2.8 mL). For the 8-arm star-shaped conjugate, 8-arm PEG maleimide (28 mg, 1.4 μmol) and stapled Ac-CGGP9 (with 7 TFA counterions; 50 mg, 14 μmol, 10 equiv. relative to 8-arm PEG) were dissolved in PBS (2.8 mL). For the short 8-arm star-shaped conjugate, short 8-arm PEG maleimide (20 mg, 2 μmol) and stapled Ac-CGGP9 (with 7 TFA counterions; 71.2 mg, 20 μmol, 10 equiv relative to short 8-arm PEG) were dissolved in PBS (4 mL). The reactions were stirred in 8 mL glass vials at room temperature for 3 h. To monitor the reactions, samples of each mixture (0.03 mL) were diluted in 1 mL HPLC eluent and analyzed by HPLC (Figure S3).

Considering that the cysteine residues of stapled Ac-CGGP9 may form disulfide bonds with cysteines on other peptide monomers, thereby yielding dimers with a molecular weight of 5.5 kDa, all conjugation mixtures were treated with the reducing agent DTT after 3 h to prevent possible disulfide-linked unconjugated peptides. Following that, reactions were dialyzed against water with 0.1% (v/v) TFA to remove the unreacted peptide. For the linear conjugate mixture, a membrane with an MWCO of 2 kDa was used to retain the ~4 kDa linear conjugate. For the star-shaped conjugates, membranes with a molecular weight cutoff (MWCO) of 3.5 kDa were used to retain these conjugates with a molecular weight ranging from ~20 to 40 kDa. Acidic conditions were selected to hinder disulfide formation and prevent supramolecular assembly during dialysis. To monitor the removal of unreacted peptide, portions of the reaction mixture (0.05 mL) were diluted in 0.95 mL of HPLC eluent for HPLC analysis. We found, however, that unconjugated peptides were not fully removed after 1 week of dialysis. Hypothesizing that the polymer conjugates may complex unreacted peptide such that it remains in the dialysis bag, ACN was added to solubilize and "release" unreacted peptide. We noted that adding 10% ACN accelerated the removal of unreacted peptide; however, when adding more than 20% v/v ACN, we started to lose the conjugate, resulting in a low yield. Purified conjugates were lyophilized and stored at −20 °C until use. Representative yields from batches of linear, 4-, 8-, and short 8-arm conjugates were 78, 75, 71, and 70%, respectively. Yields were calculated under the assumption of full conversion of the maleimide groups. We encountered some challenges during dialysis of the 8-arm star conjugates potentially due to the small size differences between the peptide and conjugates in solution, with both 8-arm star conjugates requiring longer dialysis than the others, resulting in slightly lower yields.

The peptide arm numbers on star-shaped conjugates were determined from ^{1}H NMR spectra (Figures S4−S8). PEG maleimide with different architectures and the conjugates were dissolved in D$_2$O (5 mg/mL), and proton spectra were acquired with 128 scans. The integration of the Arg δ_H resonance at 3.22 ppm, corresponding to 4H per peptide, was set to 4 in the spectra of the conjugates. The number of peptides per conjugate was calculated by comparing a polymer peak (δ = 3.37 ppm, e.g., methylene protons next to the amide carbonyl and methyl protons on linear PEG) to the peptide Arg peak in the spectra of the conjugate. We used the average number of peptide arms to estimate the molecular weight of each conjugate for calculating the conjugate concentration needed to achieve a given peptide equivalent concentration to understand the role of the polymer architecture in antimicrobial performance activity and related properties.

Secondary Structure of Stapled Ac-P9 and Corresponding Conjugates

Circular dichroism spectroscopy was run under N$_{2(g)}$ in a 0.1 cm path length quartz cell at 25 °C using a JASCO (Easton, Maryland) J-1500 CD spectrophotometer with a Peltier thermostated single-position cell holder. Peptide or conjugate samples were prepared at 0.1 mg/mL in 10 mM phosphate buffer (PB, pH = 7) or in 50% v/v TFE or 60 mM SDS to mimic the hydrophobic environment of anionic bacterial cell membranes.[33−35] Spectra were obtained in triplicate on the same

solution from 180 to 250 nm with a scanning speed of 50 nm/min and an integration time of 1 s. Mean residue ellipticity was calculated as ellipticity (θ, mdeg)/[10 × path length (l, cm) × peptide concentration (C, mol/L) × number of amino acid residues] (Figure S9). Conjugate concentrations were calculated based on the average molecular weight determined from NMR spectra, inclusive of TFA counterions on each cationic Lys and Arg residues, as well as protons on each anionic Glu residue.

Antimicrobial Activity of Stapled Ac-P9 and Corresponding Conjugates

The antimicrobial activity of peptides and conjugates was evaluated against a well-characterized multidrug-resistant (MDR) clinical isolate, *Klebsiella pneumoniae* BL13802,[33,36,37] using the metabolic indicator dye alamarBlue to quantify bacterial viability/survival, as previously described.[33,38−41] Briefly, logarithmic-phase bacteria (grown in LB medium to an OD$_{600}$ of ~0.6) were diluted in RPMI medium and combined in a 1:1 ratio with medium alone or containing peptides/conjugates in the wells of a 96-well plate (200 μL total volume with ~2.5 × 10^5 CFU/mL and final peptide equivalent concentrations of 200 or 100 μM). Wells containing only RPMI medium were included in each experiment as a sample blank. After exposure (2 h at 37 °C with shaking, 270 rpm), triplicates of all samples (50 μL per replicate) were re-plated into individual wells of a clear-bottom, black-wall microplate. An equal volume of 2× LB medium was then added to every well, followed by 10 μL of the alamarBlue reagent. The sample plate was protected from light with foil and incubated at 37 °C (without shaking) until the untreated control, bacteria exposed to media alone, began to demonstrate a colorimetric change (approximately 2−3 h). At this point, the fluorescence (excitation 530 nm; emission 580 nm) of each well was measured using a VICTOR Nivo multimode plate reader by PerkinElmer. In some cases, multiple reads were taken to ensure that resultant data sets were within the linear range of the instrument's detector for this assay (<6 million relative fluorescence units, RFU). To calculate percent bacterial survival, blank-corrected sample signals were divided by those obtained from the untreated control.

Hemolysis of Stapled Ac-CGGP9 and Corresponding Conjugates

Research utilizing human-derived materials was approved by the University of Virginia Institutional Review Board for Health Sciences Research (IRB-HSR; protocol #13909). Red blood cells (RBCs), isolated from Ficoll−Paque separations of human whole blood, were diluted 1:10 with PBS (pH 7.4) in a 50 mL centrifuge tube. The solution was mixed by inversion and centrifuged at 500g for 10 min at room temperature. RBCs were washed with 1× PBS twice as much as above and then diluted 1:20 (v/v, 5% final) in RPMI medium (without phenol red) that was supplemented with low-endotoxin BSA (1% final). Medium lacking phenol red was used since the color imparted by this pH indicator interferes with the absorbance measurement that quantifies hemolysis. Processed RBCs (180 μL) were combined with test peptides/conjugates (20 μL, 2 mM peptide equivalent) in triplicate in the wells of a round-bottom microplate. Included in each assay were also samples containing RBCs together with the hemolytic peptide melittin (positive control), media alone (negative control and analytical blank), H$_2$O (vehicle control), or Triton X-100 (1% final; complete hemolysis). Following incubation (1 h at 37 °C), the assay plate was centrifuged at 500g for 5 min. Supernatants (100 μL) were transferred to a fresh flat-bottom microplate, and sample absorbance was measured at 540 nm using a VICTOR Nivo plate reader. To calculate percent hemolysis, blanked sample absorbance readings were divided by those obtained from RBCs exposed to Triton X-100.

Proteolytic Stability of Stapled Ac-P9 and the Corresponding Conjugates

Stock solutions of Proteinase K (5 μM, 0.14 mg/mL) and the tested peptides/conjugates (250 μM peptide equivalent) were prepared in either RPMI medium or 1× PBS (pH = 7.4) right before use. The mass concentrations of the stapled Ac-P9 and Ac-CGGP9, as well as

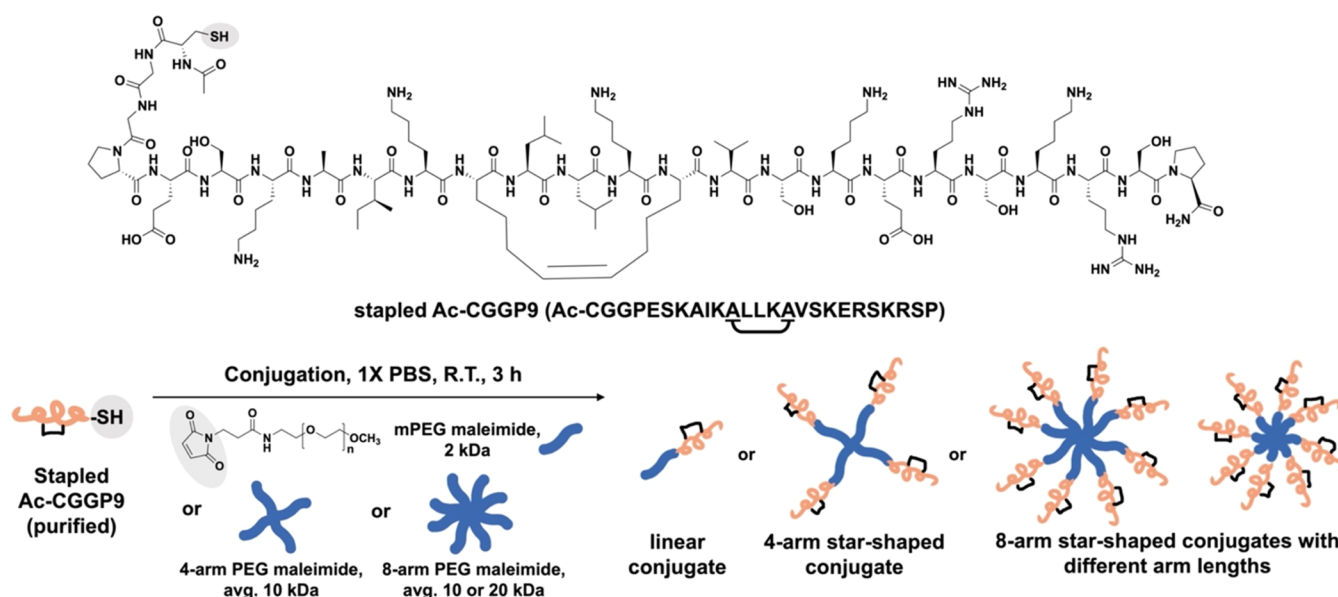**stapled Ac-CGGP9 (Ac-CGGPESKAIKALLKAVSKERSKRSP)**

Figure 1. Conjugation scheme, in which the thiol-terminated AMP stapled Ac-CGGP9 was appended to maleimide-functionalized linear and star-shaped PEG, using 1.1 or 1.25 equiv of peptides relative to the maleimide amount on linear and star-shaped polymers, respectively.

the linear, 4-, 8-, and short 8-arm star-shaped conjugate stock solutions were 0.84, 0.89, 1.39, 1.78, 1.57, and 1.23 mg/mL, respectively. Stock solutions of peptides/conjugates (0.6 mL) were mixed with a Proteinase K stock solution (0.6 mL) and filtered into a 2 mL HPLC sample vial before characterization. HPLC was used to monitor degradation by injecting sample mixtures (100 μL) after incubation in the presence or absence of Proteinase K for 0.5 1, 2, and 24 h. Control samples were prepared by diluting the corresponding stock solution (0.6 mL) with an RPMI medium or PBS alone (0.6 mL). The fractions of peak area were calculated from HPLC traces by comparing the peak area of the control samples to those treated with Proteinase K. To verify that Proteinase K was still functional after 24 h of incubation, additional peptide (0.2 mg stapled Ac-P9) was added into the reaction after the prior 24 h incubation. The mixture was filtered before injection, and HPLC was used to monitor the process at 10, 40, and 70 min after spiking in additional peptide.

RESULTS AND DISCUSSION

Synthesis of Stapled Ac-CGGP9-PEG Conjugates

For the AMP component of our conjugates in this study, we selected a previously studied antimicrobial peptide, called P9, which is derived from the C-terminus of the human chemokine CXCL10.[33,42] To help retain the helical structure of this chemokine-derived peptide, a hydrocarbon staple and N-terminal acetyl (Ac) cap are installed.[33] The resulting peptide, stapled Ac-P9, is active against a range of antibiotic-resistant bacterial isolates and does not exhibit significant hemolysis at concentrations commensurate with bacterial killing. As this helical peptide resembles many traditional membrane-disrupting AMPs in its amphipathic character,[5] we envision that the design rules established here will be useful to conceiving other useful AMP−polymer conjugates.

For the conjugation reactions, we selected thiol-maleimide "click" chemistry since the multiple amines on the lysine residues of stapled Ac-P9 would preclude site-selective conjugation with activated esters (e.g., N-hydroxysuccinimide (NHS) esters). Solid-phase peptide synthesis was used to prepare stapled Ac-CGGP9 with an N-terminal cysteine and a double glycine linker between the AMP and cysteine residues to ensure the availability of the cysteine thiol for the reaction

with the maleimide groups at the PEG chain ends (Figure 1). Following solid-phase synthesis, the thiol-functionalized AMP-stapled Ac-CGGP9 was isolated to >99% purity by preparative-scale reverse-phase HPLC (Figures S1 and S2). In designing a series of conjugates that vary in the number of peptide-functionalized arms but have similar compositions, we opted for commercially available linear, as well as 4- and 8-arm star-shaped PEG maleimides with arm lengths of ~2−2.5 kDa (similar to the molecular weight of the 2.5 kDa peptide) for a reaction with thiol-functionalized AMPs. An additional conjugate was prepared by holding the arm number constant at 8 but shortening the PEG arm length to 1.25 kDa.

Conjugation reactions were performed at room temperature for 3 h with excess peptide (1.1 equiv relative to maleimide groups on linear PEG or 1.25 equiv relative to maleimide groups on all star-shaped PEGs). Monitoring by HPLC, we noticed that most of the peptide reacted in the 1st hour, after which excess thiol-containing peptide started to form disulfide-linked peptide dimers (Figure S3). Thus, before dialysis, we treated mixtures with DTT to reduce the disulfides and restore the larger size difference between the unreacted peptide and conjugates. A mixture of acidic water and ACN was chosen for the dialysis to limit aggregation and disulfide formation. To minimize the loss of prepared conjugates, HPLC was used to monitor the process and stop dialysis when the fraction of the unreacted peptide in the mixture was lower than 5% (Figure S3). SEC was also used to analyze conjugate purity: all conjugates were found to be >95% pure (Figure 2). We note that the SEC traces of the star-shaped conjugates contained shoulders, consistent with analogous shoulders seen in SEC traces of PEG maleimides alone. The yields of linear, 4-, 8-, and short 8-arm conjugates were 78, 75, 71, and 70%, respectively.

To determine the average number of peptide arms attached and, therefore, the peptide content (wt % peptide) of each conjugate, we used NMR spectroscopy (Figures S4−S8). The linear polymer reacted quantitatively with the peptide, as assessed by comparing the integrations of the Arg δ_H resonance at 3.22 ppm (4 protons per peptide) and the PEG maleimide
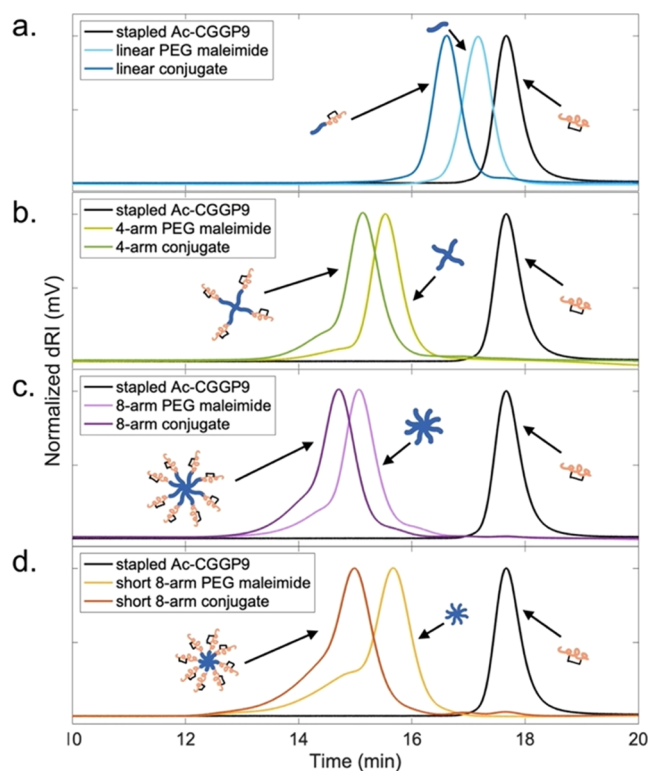
Figure 2. SEC traces of stapled Ac-CGGP9 (black), PEG maleimide with different architectures (light colors), and the corresponding conjugates (dark colors): (a) linear; (b) 4-arm star-shaped conjugate; (c) 8-arm star-shaped conjugate; and (d) short 8-arm star-shaped conjugate.

proton resonances at 3.37 ppm (2 methylene protons next to the amide carbonyl and 3 methyl protons at the chain end per polymer) in the conjugate spectra. Both 8-arm conjugates were almost fully functionalized, with the peptide contents calculated from NMR spectroscopy very close to the targeted values. The 4-arm conjugate, however, was found to average only 2.8 peptide-functionalized arms, and neither a higher molar ratio nor a new batch of PEG maleimide improved the conversion of the conjugation reaction, possibly due to steric hindrance or assembly formation during conjugation that limited the availability of unconjugated peptides. As such, the

4-arm star conjugate contained 44 wt % peptide, slightly lower than the 53 wt % target (Table 1). While noting this difference from the intended composition, the linear, 4-arm, and 8-arm conjugates with ~2−2.5 kDa arms have peptide contents that fall within a comparable peptide composition range (44−58 wt %).

Secondary Structure

Given that the helical secondary structure of stapled Ac-P9 is essential to its antimicrobial activity,[33] we used circular dichroism (CD) spectroscopy to assess the secondary structure of the conjugates to verify that the helical structure is retained upon conjugation. To better understand how arm number and length affect the helical content in different environments, we acquired CD spectra in 50% TFE, an organic solvent that can promote helicity by enhancing the peptide H-bonding,[34,43] and 60 mM SDS, an anionic bacterial membrane mimetic solution,[35] in addition to 10 mM PB (Figure S9). The spectra of all conjugates, in all 3 solutions, displayed characteristic features of α-helical peptides (λ_{min} at 206 and 222 nm) and were similar to the peptide alone with little-to-no difference in mean residue ellipticity at these minima. These observations suggest that conjugation to polymers with different architectures does not disrupt the α-helical secondary structure important for the antimicrobial function of stapled Ac-P9.

Solution Behavior

Owing to the chemically distinct nature of stapled Ac-P9 and PEG, it is quite possible that the conjugates will assemble in solution. To ascertain whether the conjugates assemble in solution and, if so, how this impacts the presentation of constituent AMPs, we measured the ζ-potential, size, and morphology of the AMP alone, as well as of the linear and star-shaped conjugates. We note that for evaluating solution behavior and antimicrobial effects, we used stapled Ac-P9 rather than the cysteine-functionalized stapled Ac-CGGP9 peptide due to the propensity of unconjugated cysteines to form disulfides. For these measurements, we held the peptide equivalent concentrations constant at 200 μM in 10 mM PBS, a buffer that limits salt interference with ζ-potential measurements and TEM imaging.

As electrostatic interactions between the cationic AMP and anionic bacterial membranes are likely important for antimicrobial activity, we first determined and compared the ζ-potentials of the conjugates (Figure 3a). While the AMP

Table 1. Peptide Content of Linear and Star-Shaped Stapled P9-PEG Conjugates

	stapled Ac-P9	linear conjugate	4-arm conjugate	8-arm conjugate	short 8-arm conjugate
Average AMP number [a]	1	1	2.8	7.4	7.3
PEG MW per arm (kDa) [b]	-	2	2.5	2.5	1.25
AMP/conjugate MW (kDa) [c]	2.5	4.7	17.7	40.5	30.2
Target AMP content (wt. %) [d]	100	58	53	53	69
Actual AMP content (wt. %) [e]	100	58	44	51	67

[a]Average AMPs per molecule was determined by ^{1}H NMR spectra. [b]Number-average molecular weight as reported by the manufacturer. [c]Calculated as the average AMP number × AMP MW + PEG MW per arm × arm number. [d]Calculated assuming full conversion of maleimides in the conjugation. [e]Calculated as the average AMP number × AMP MW/conjugate MW.
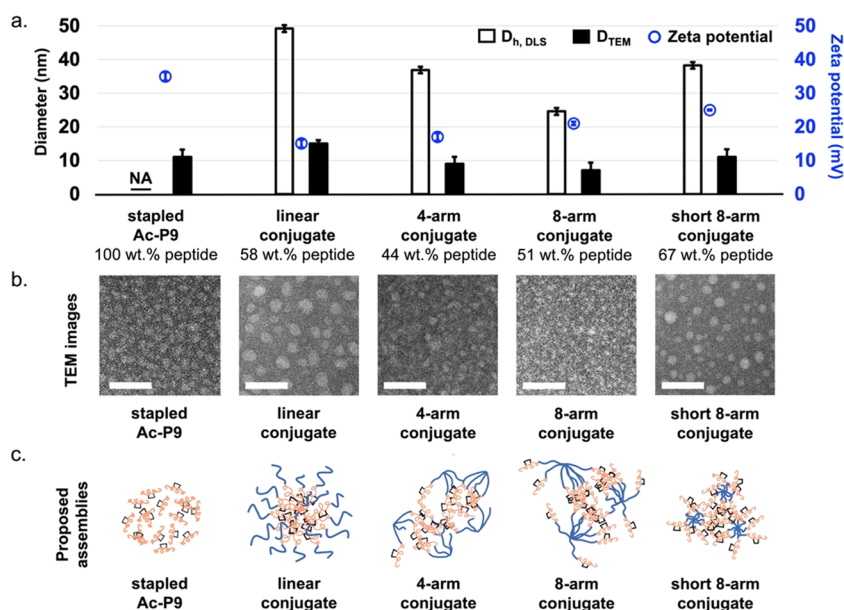
Figure 3. ζ-potential, size, and morphology of stapled Ac-P9 and its conjugates at a constant concentration of 200 μM peptide equivalent. (a) ζ-potential (circles) and size (bars) of stapled Ac-P9 alone and conjugates in 10 mM PBS. We report the Z-average hydrodynamic diameter from DLS ($D_{h,\ DLS}$) and the average diameter from TEM images (D_{TEM}). Error bars represent the standard deviation. (b) Representative TEM images of stapled Ac-P9 and conjugates in 10 mM PBS, showing more distinctly spherical assemblies of the linear and short 8-arm conjugate than from the other conjugates. Scale bar = 50 nm. (c) Proposed assembled structures. Stapled Ac-P9 is soluble or forms very small aggregates in solution. The low ζ-potential and larger size of the spherical particles formed from the linear conjugates suggest the formation of micelles with PEG coronas partially sequestering the peptide within the cores. The 4- and 8-arm star-shaped conjugates with 2.5 kDa PEG arms have lower peptide contents and form structures that likely still involve small-peptide aggregates connecting multiple conjugates into particles. As seen with the short 8-arm conjugate, shortening the PEG arms increases the peptide content and restores the spherical morphology, though the high ζ-potential is consistent with the presentation of peptides at the particle surface, where electrostatic repulsion may limit particle size.

alone yielded a ζ-potential of +35 mV, consistent with its cationic character, that of the linear conjugate was just +15 mV, suggesting that the PEG chains partially shield the AMP from solution. ζ-potential trended upward upon increasing the number of peptide-functionalized arms, consistent with the increasing local concentration of peptides. The 8-arm star-shaped conjugate exhibited a ζ-potential of +21 mV and shortening the PEG arms to 1.25 kDa produced a further increase in ζ-potential to +25 mV.

With ζ-potential measurements suggesting that the polymers at least partially shield the cationic AMP, we next determined the size and morphology of the conjugates in 10 mM PBS (pH = 7.4) using dynamic light scattering (DLS) (Figures 3a and S10−S12) and transmission electron microscopy (TEM) (Figures 3b, S13, and S14). By DLS, the hydrodynamic diameter of the structures formed from the linear conjugate was 49 nm. We were unable to obtain reliable particle size data for the peptide alone, possibly due to the lack of assembly at a lower concentration relative to those reached as a result of drying on TEM grids. While linear PEG alone produced no observable features in TEM images (Figure S13c), images of the linear peptide−polymer conjugate revealed spherical nanostructures averaging ca. 15 nm in diameter (Figures 3b and S13d). For comparison, TEM images of stapled Ac-P9 alone showed a distribution of smaller nanostructures ca. 11 nm in diameter.

The 4- and 8-arm star-shaped conjugates with 2.5 kDa arms formed smaller structures that were less distinct, with lower resolution and contrast in the TEM images than those from the linear conjugate. Hydrodynamic diameters determined from DLS for the linear, 4-arm, and 8-arm star-shaped conjugates

were 49, 37, and 25 nm, respectively (Figure 3a and Table S1). TEM images reinforced the finding that these 4- and 8-arm star-shaped conjugates assembled into smaller structures, with the average diameters of the linear, 4-arm, and 8-arm conjugates being 15, 9, and 7 nm, respectively (Figures 3b and S13g,h). TEM imaging also revealed the distinctly less spherical morphology of these star-shaped conjugates relative to the linear conjugate, which may arise either from the high local concentration of peptide on the star-shaped materials or their slightly lower peptide content (44−51 wt % peptide on the star-shaped conjugates vs 58 wt % peptide on the linear conjugate).

Shortening the PEG arm length from 2.5 to 1.25 kDa on the 8-arm conjugate increased both the particle size and the spherical nature of the resulting particles. The increase in particle size, from an average hydrodynamic diameter of 25 nm for the long-arm star to 38 nm for the short-arm star by DLS (Figure 3a and Table S1) and from an average diameter of 9 to 11 nm by TEM (Figures 3b and S13e,f,h), may be due to the increase in peptide content, from 51 to 67 wt %, that accompanies the decrease in PEG arm length. The short 8-arm star-shaped and linear conjugate have similar spherical morphologies, which may allow us to ascribe these more distinct spherical morphologies to their slightly higher peptide contents (58 and 67 wt % peptides) compared to the 4-arm and 8-arm star-shaped conjugates with 2.5 kDa arms (44 and 51 wt % peptide). Further, the higher ζ-potential of the short 8-arm conjugate compared to the linear conjugate (+25 mV vs +15 mV) may explain the smaller particle size of the short 8-arm conjugate, as the electrostatic repulsion between the
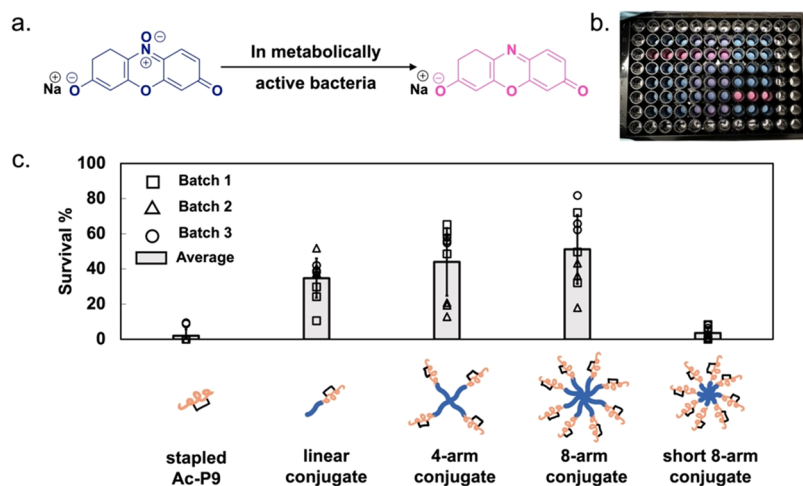
Figure 4. AlamarBlue assay was used to test the antimicrobial activity of stapled Ac-P9 and its conjugates against *K. pneumoniae*. (a) Reduction of the alamarBlue reagent by metabolically active bacteria yields a pink, fluorescent product. (b) Photograph of a 96-well plate showing wells with pink, purple, and blue solutions indicative of high, medium, and low amounts, respectively, of viable bacteria. (c) Bacterial survival (%) after treatment with the indicated AMP or conjugate (peptide equiv. concentration = 100 μM in RPMI medium). Three independently prepared batches of materials (square, triangle, and circle) were tested in triplicate. Results are plotted for each batch and the bars indicate the average. Error bars represent the standard deviation. The illustrations are intended to indicate the different conjugate formulations rather than to imply their structures in solution.

cationic peptide, presented at higher density at the surface of short 8-arm conjugate assemblies, may limit particle size.

Taking together the ζ-potential, size, and morphology of the conjugates, we propose possible assembled structures (Figure 3c). Comparing the featureless TEM images of PEG alone (Figure S13) to those showing aggregates of the unconjugated peptide suggests that the hydrophobic content in the peptide may be driving assembly of the conjugates in solution.[28,44,45] Yet, when not subject to the high peptide concentrations reached upon drying on TEM grids, the lack of reliable DLS data and visibly clear solutions lead us to conclude that the peptide is soluble or exists in very small aggregates at 200 μM. The low ζ-potential and spherical morphology of the linear conjugate point to assembly into nanostructures with peptide cores and polymer shells. We hypothesize that the smaller, less distinct assemblies formed from 4- and 8-arm star-shaped conjugates with 2.5 kDa arms are still held together by a peptide core but that the slightly lower peptide content in these samples results in looser peptide assemblies, connecting these conjugates into more diffuse particles. By DLS, the intensity-average size distribution of the 8-arm conjugate (Figure S11) showed a higher fraction of smaller single-chain-sized particles compared to the 4-arm conjugate. We speculate that this was due to the slightly higher ζ-potential of the 8-arm versus the 4-arm conjugate and is consistent with the higher local concentration of cationic peptide, leading to charge repulsion between conjugate molecules. Increasing the peptide content by reducing PEG arm length in the short 8-arm conjugate restores the spherical morphology, yet these particles are smaller than those formed from the linear conjugate. For both long- and short 8-arm conjugates, the peptide arms may still be collecting the conjugates into particles, but electrostatic repulsion between the cationic peptides present at high local concentrations may be limiting particle size (Figures S11, S13, and S14).

Bactericidal Activity against *K. pneumoniae*

The ability of prepared conjugates to kill an MDR *K. pneumoniae* clinical isolate (i.e., BL13802) was evaluated

using the viability reagent alamarBlue.[38,46] When alive, bacteria reduce the alamarBlue reagent to a fluorescent product. Normalization of this signal, relative to that produced in untreated bacteria, yields a percentage of surviving bacteria (Figure 4a).[33] Similar to our solution property studies, we held peptide concentrations constant to show how arm number and arm length affect antimicrobial activity. We tested two peptide equivalent concentrations (i.e., 100 and 200 μM) that highlight differences among the conjugates (Figure S15). The antimicrobial effects at 100 μM peptide equivalent are shown in Figure 4c on a linear scale and in Figure S15a on a log scale. Of note, we repeated these measurements with three independently synthesized batches of each material, thereby highlighting the reproducibility of synthesis methodologies and strengthening the rigor of our results.

Stapled peptide Ac-P9 killed most of the bacteria (96%). The linear conjugate only killed ~50% of treated organisms, consistent with the lower ζ-potential and corresponding reduction in peptide availability. We hypothesized that increasing the arm number would increase activity by elevating the local concentration of the peptide; however, we did not observe significant increases in bacterial killing by the 4- and 8-arm star-shaped conjugates with 2.5 kDa arms. We found that these conjugates also had less-defined nanostructures in solution. Thus, the low antimicrobial activity of conjugates with longer arms may arise from insufficient local concentrations of the peptide and/or shielding by PEG. The increase in ζ-potential of the 8-arm conjugate compared to the 4-arm analogue (attributed to a higher local concentration of the peptide arms) seemed to be insufficient to support greater antimicrobial activity.

Shortening the length of the PEG arms on the 8-arm conjugate to 1.25 kDa produced conjugate molecules with antimicrobial activity rivaling that of the free peptide (96% bacterial killing in both cases). We attribute this retention of activity to the higher local peptide concentration both at the molecular level and when the peptides likely collect into spherical assemblies with high ζ-potential. While the activity of
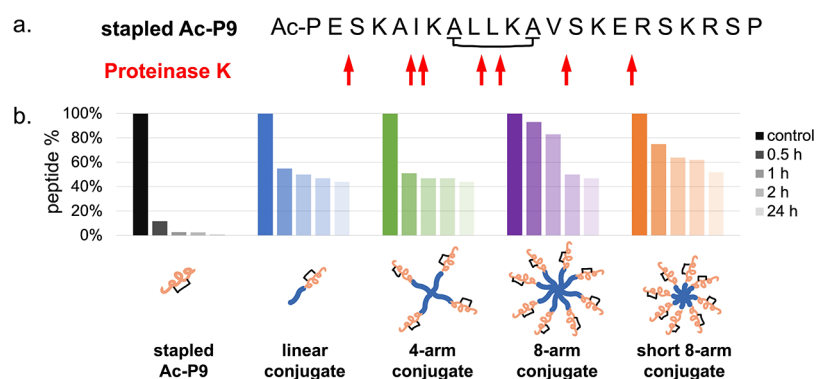
Figure 5. Protease resistance of stapled Ac-P9 and conjugates against Proteinase K in RPMI medium. (a) The primary amino acid sequence of stapled peptide Ac-P9 with predicted cleavage sites indicated by red arrows (sites identified using Peptide Cutter).[47] (b) Summary of intact peptide/conjugate fraction after incubation with Proteinase K for 0.5, 1, 2, and 24 h. Fractions were calculated from the peak area ratio of the HPLC traces at each time point relative to the untreated control (Table S2). The illustrations are intended to indicate the different conjugate formulations rather than to imply their structures in solution.

the linear, 4-arm, and 8-arm conjugates showed some variation between different batches and experimental replicates, the short 8-arm conjugates consistently exhibited robust bacterial killing.

Hemolysis

We next measured human red blood cell (RBC) hemolysis caused by the free peptide and conjugates at a standardized peptide concentration. While our previous study showed that stapled peptide P9 does not induce significant hemolysis at 50 μM, here, we increased the peptide concentration to 200 μM. Encouragingly, neither the free peptide nor any conjugate caused significant hemolysis under the conditions examined (<5%; Figure S16), suggesting that varying the architecture of the conjugates did not introduce hemolytic tendency compared to the unconjugated peptide. In particular, the short 8-arm conjugate, which showed antimicrobial activity similar to that of the stapled Ac-P9, was not hemolytic, regardless of its assembly in solution.

Protease Resistance

One of the most significant motivations for conjugating AMPs to polymers is to improve the protease resistance of the constituent AMP(s). Typically, this occurs by the polymer blocking proteases from accessing the AMP. Our solution assembly studies suggested that the polymers may partially shield peptides, so we sought to determine how this would translate to preventing proteolytic degradation. For these studies, we selected Proteinase K as a model protease, as it is predicted to cleave stapled Ac-P9 at multiple sites (indicated by the red arrows in Figure 5a).[47] To monitor degradation, we used HPLC to track the fraction of intact peptide by comparing the peptide/conjugate peak area before and after incubation with Proteinase K under the same conditions used for measuring antimicrobial activity.

In contrast to the free peptide, which was almost fully degraded after incubation with Proteinase K for just 30 min, all peptide–polymer conjugates showed improved stability (Figures 5b and S17−S21). The degradation of conjugates slowed after 2 h, and all conjugates retained more than 40% intact peptide after 24 h incubation with Proteinase K. In particular, the high-density 8-arm structures with longer arms preserved ca. 80% of the conjugated peptide after 1 h, which was much higher than the linear (50% intact peptide) and 4-arm (47% intact peptide) conjugates. Notably, the short 8-arm

conjugate, which exhibited comparable antimicrobial activity as free peptide, provided the highest stability among all conjugates after the 24 h incubation, preserving more than 50% of the conjugated peptides, possibly due to the assembled structure with high peptide density providing steric hindrance that slows degradation.

To verify that Proteinase K was still active after 24 h and that a loss of enzymatic activity did not account for the increased protease resistance of the conjugates, more stapled Ac-P9 peptide was added to the free peptide mixture after 24 h incubation (Figure S17). The stapled Ac-P9 peak increased initially after the spike and then decreased, demonstrating that Proteinase K was indeed still functional after 24 h. This observation reinforces the finding that conjugated peptides exhibit higher protease resistance than the free peptide. Similar results were obtained in 1× PBS (Table S3 and Figures S22−S27).

We suspect that enhanced protease resistance upon conjugation arises from a combination of PEG shielding the peptides from proteases and the high-density presentation of peptides within the star-shaped conjugate assemblies, hindering access to cleavage sites. Indeed, Gianneschi and co-workers reported that high-density displays of the peptide on comb-like peptide–polymer conjugates imparted proteolytic stability.[48] Together with the antimicrobial activity data, these findings point to a high-density presentation of AMPs on polymers as a favorable molecular design that strikes a good balance between shielding the AMP from proteolytic degradation without compromising antimicrobial activity.

■ CONCLUSIONS

In this work, we prepared a series of peptide–polymer conjugates from the AMP stapled Ac-P9 and linear/star-shaped PEG, varying in arm number and length. To better understand the structure−property−performance relationships, we conducted our investigations at a constant peptide equivalent concentration. Both polymer architecture and peptide content seemed to influence the assembly in solution, since while the ζ-potential trended upward with an increasing peptide arm number, slight differences in peptide content (imposed by the conversion of peptide conjugation reactions and availability of commercial PEG at a given molecular weight) impacted the resulting morphology. Decreasing the PEG arm length increased the peptide content and the local

concentration of peptides, resulting in small, spherical assemblies with high ζ-potential. While designing structures with higher activity can come at the expense of cell viability and protease resistance, we found that the short 8-arm conjugate exhibited high bactericidal activity, low hemolysis, and enhanced resistance against proteolytic degradation. Going forward, other synthetic strategies (e.g., grafting-from or grafting-through) and architectures (e.g., comb-like or hyperbranched) that support high-density peptide presentation on neutral hydrophilic polymers are a promising future direction for the molecular design of AMP−polymer conjugates.

■ ASSOCIATED CONTENT

ⓈⒾ Supporting Information

The Supporting Information is available free of charge at https://pubs.acs.org/doi/10.1021/acspolymersau.3c00026.

Additional experimental procedures, characterization details, and data (PDF)

Special Issue Paper

Published as part of *ACS Polymers Au* virtual special issue "2023 Rising Stars".

■ AUTHOR INFORMATION

Corresponding Author

Rachel A. Letteri − *Department of Chemical Engineering, University of Virginia, Charlottesville, Virginia 22903, United States*; ◉ orcid.org/0000-0002-2919-203X; Email: rl2qm@virginia.edu

Authors

Zixian Cui − *Department of Chemical Engineering, University of Virginia, Charlottesville, Virginia 22903, United States*

Matthew A. Crawford − *Division of Infectious Diseases & International Health, Department of Medicine, University of Virginia, Charlottesville, Virginia 22908, United States*; ◉ orcid.org/0000-0003-0404-0061

Blake A. Rumble − *Division of Infectious Diseases & International Health, Department of Medicine, University of Virginia, Charlottesville, Virginia 22908, United States*

Megan M. Krogh − *Division of Infectious Diseases & International Health, Department of Medicine, University of Virginia, Charlottesville, Virginia 22908, United States*

Molly A. Hughes − *Division of Infectious Diseases & International Health, Department of Medicine, University of Virginia, Charlottesville, Virginia 22908, United States*

Complete contact information is available at:
https://pubs.acs.org/10.1021/acspolymersau.3c00026

Notes

The authors declare no competing financial interest.

■ ACKNOWLEDGMENTS

■ REFERENCES

(1) O'Neill, J. Tackling Drug-Resistant Infections Globally: Final Report and Recommendations 2016 https://amr-review.org/sites/default/files/160518_Final%20paper_with%20cover.pdf (accessed November 20, 2023).

(2) Lu, J.; Sheldenkar, A.; Lwin, M. O. A Decade of Antimicrobial Resistance Research in Social Science Fields: A Scientometric Review. *Antimicrob. Resist. Infect. Control* **2020**, *9* (1), 178.

(3) Mookherjee, N.; Anderson, M. A.; Haagsman, H. P.; Davidson, D. J. Antimicrobial Host Defence Peptides: Functions and Clinical Potential. *Nat. Rev. Drug Discovery* **2020**, *19* (5), 311−332.

(4) Lazzaro, B. P.; Zasloff, M.; Rolff, J. Antimicrobial Peptides: Application Informed by Evolution. *Science* **2020**, *368* (6490), No. eaau5480.

(5) Kumar, P.; Kizhakkedathu, J. N.; Straus, S. K. Antimicrobial Peptides: Diversity, Mechanism of Action and Strategies to Improve the Activity and Biocompatibility in Vivo. *Biomolecules* **2018**, *8* (1), 4.

(6) Shi, G.; Kang, X.; Dong, F.; Liu, Y.; Zhu, N.; Hu, Y.; Xu, H.; Lao, X.; Zheng, H. DRAMP 3.0: An Enhanced Comprehensive Data Repository of Antimicrobial Peptides. *Nucleic Acids Res.* **2022**, *50* (D1), D488−D496.

(7) Oishi, S.; Ito, S.; Nishikawa, H.; Watanabe, K.; Tanaka, M.; Ohno, H.; Izumi, K.; Sakagami, Y.; Kodama, E.; Matsuoka, M.; Fujii, N. Design of a Novel HIV-1 Fusion Inhibitor That Displays a Minimal Interface for Binding Affinity. *J. Med. Chem.* **2008**, *51* (3), 388−391.

(8) Li, W.; Separovic, F.; O'Brien-Simpson, N. M.; Wade, J. D. Chemically Modified and Conjugated Antimicrobial Peptides against Superbugs. *Chem. Soc. Rev.* **2021**, *50* (2012), 4932−4973.

(9) Matthyssen, T.; Li, W.; Holden, J. A.; Lenzo, J. C.; Hadjigol, S.; O'Brien-Simpson, N. M. The Potential of Modified and Multimeric Antimicrobial Peptide Materials as Superbug Killers. *Front. Chem.* **2022**, *9*, 795433.

(10) Martin-Serrano, Á.; Gómez, R.; Ortega, P.; La Mata, F. J. D. Nanosystems as Vehicles for the Delivery of Antimicrobial Peptides (AMPs). *Pharmaceutics* **2019**, *11*, No. 448, DOI: 10.3390/pharmaceutics11090448.

(11) Tang, Z.; Ma, Q.; Chen, X.; Chen, T.; Ying, Y.; Xi, X.; Wang, L.; Ma, C.; Shaw, C.; Zhou, M. Recent Advances and Challenges in Nanodelivery Systems for Antimicrobial Peptides (AMPs). *Antibiotics* **2021**, *10* (8), 990 DOI: 10.3390/antibiotics10080990.

(12) Sun, H.; Hong, Y.; Xi, Y.; Zou, Y.; Gao, J.; Du, J. Synthesis, Self-Assembly, and Biomedical Applications of Antimicrobial Peptide-Polymer Conjugates. *Biomacromolecules* **2018**, *19* (6), 1701−1720.

(13) Cui, Z.; Luo, Q.; Bannon, M. S.; Gray, V. P.; Bloom, T. G.; Clore, M. F.; Hughes, M. A.; Crawford, M. A.; Letteri, R. A. Molecular Engineering of Antimicrobial Peptide (AMP)-Polymer Conjugates. *Biomater. Sci.* **2021**, *9* (15), 5069−5091.

(14) Joralemon, M. J.; McRae, S.; Emrick, T. PEGylated Polymers for Medicine: From Conjugation to Self-Assembled Systems. *Chem. Commun.* **2010**, *46* (9), 1377−1393.

(15) Imura, Y.; Nishida, M.; Ogawa, Y.; Takakura, Y.; Matsuzaki, K. Action Mechanism of Tachyplesin I and Effects of PEGylation. *Biochim. Biophys. Acta* **2007**, *1768* (5), 1160−1169.

(16) Imura, Y.; Nishida, M.; Matsuzaki, K. Action Mechanism of PEGylated Magainin 2 Analogue Peptide. *Biochim. Biophys. Acta* **2007**, *1768* (10), 2578−2585.

(17) Li, T.; Yang, N.; Teng, D.; Mao, R.; Hao, Y.; Wang, X.; Wang, J. C-Terminal Mini-PEGylation of a Marine Peptide N6 Had Potent Antibacterial and Anti-Inflammatory Properties against *Escherichia Coli* and Salmonella Strains in Vitro and in Vivo. *BMC Microbiol* **2022**, *22* (1), 128.

(18) Kaur, N.; Dilawari, R.; Kaur, A.; Sahni, G.; Rishi, P. Recombinant Expression, Purification and PEGylation of Paneth Cell Peptide (Cryptdin-2) with Value Added Attributes against Staphylococcus Aureus. *Sci. Rep.* **2020**, *10* (1), No. 12164.

(19) Morris, C. J.; Beck, K.; Fox, M. A.; Ulaeto, D.; Clark, G. C.; Gumbleton, M. Pegylation of Antimicrobial Peptides Maintains the Active Peptide Conformation, Model Membrane Interactions, and Antimicrobial Activity While Improving Lung Tissue Biocompatibility Following Airway Delivery. *Antimicrob. Agents Chemother.* **2012**, *56* (6), 3298−3308.

(20) Lam, S. J.; O'Brien-Simpson, N. M.; Pantarat, N.; Sulistio, A.; Wong, E. H. H.; Chen, Y. Y.; Lenzo, J. C.; Holden, J. A.; Blencowe, A.; Reynolds, E. C.; Qiao, G. G. Combating Multidrug-Resistant Gram-Negative Bacteria with Structurally Nanoengineered Antimicrobial Peptide Polymers. *Nat. Microbiol.* **2016**, *1*, 16162.

(21) Pranantyo, D.; Xu, L. Q.; Kang, E. T.; Mya, M. K.; Chan-Park, M. B. Conjugation of Polyphosphoester and Antimicrobial Peptide for Enhanced Bactericidal Activity and Biocompatibility. *Biomacromolecules* **2016**, *17* (12), 4037−4044.

(22) Chen, Y.; Yu, L.; Zhang, B.; Feng, W.; Xu, M.; Gao, L.; Liu, N.; Wang, Q.; Huang, X.; Li, P.; Huang, W. Design and Synthesis of Biocompatible, Hemocompatible, and Highly Selective Antimicrobial Cationic Peptidopolysaccharides via Click Chemistry. *Biomacromolecules* **2019**, *20* (6), 2230−2240.

(23) Shirbin, S. J.; Insua, I.; Holden, J. A.; Lenzo, J. C.; Reynolds, E. C.; O'Brien-Simpson, N. M.; Qiao, G. G. Architectural Effects of Star-Shaped "Structurally Nanoengineered Antimicrobial Peptide Polymers" (SNAPPs) on Their Biological Activity. *Adv. Healthcare Mater.* **2018**, *7* (21), No. 1800627.

(24) Lu, C.; Quan, G.; Su, M.; Nimmagadda, A.; Chen, W.; Pan, M.; Teng, P.; Yu, F.; Liu, X.; Jiang, L.; Du, W.; Hu, W.; Yao, F.; Pan, X.; Wu, C.; Liu, D.; Cai, J. Molecular Architecture and Charging Effects Enhance the In Vitro and In Vivo Performance of Multi-Arm Antimicrobial Agents Based on Star-Shaped Poly(l -lysine). *Adv. Ther.* **2019**, *2*, 1900147.

(25) Wong, E. H. H.; Khin, M. M.; Ravikumar, V.; Si, Z.; Rice, S. A.; Chan-Park, M. B. Modulating Antimicrobial Activity and Mammalian Cell Biocompatibility with Glucosamine-Functionalized Star Polymers. *Biomacromolecules* **2016**, *17* (3), 1170−1178.

(26) Zhang, G.; Han, B.; Lin, X.; Wu, X.; Yan, H. Modification of Antimicrobial Peptide with Low Molar Mass Poly(Ethylene Glycol). *J. Biochem.* **2008**, *144* (6), 781−788.

(27) Costanza, F.; Padhee, S.; Wu, H.; Wang, Y.; Revenis, J.; Cao, C.; Li, Q.; Cai, J. Investigation of Antimicrobial PEG-Poly(Amino Acid)S. *RSC Adv.* **2014**, *4* (4), 2089−2095.

(28) Zhang, Y.; Guan, T.; Han, G.; Guo, T.; Zhang, W. Star Block Copolymer Nanoassemblies: Block Sequence Is All-Important. *Macromolecules* **2019**, *52* (2), 718−728.

(29) Laaser, J. E.; Jiang, Y.; Petersen, S. R.; Reineke, T. M.; Lodge, T. P. Interpolyelectrolyte Complexes of Polycationic Micelles and Linear Polyanions: Structural Stability and Temporal Evolution. *J. Phys. Chem. B* **2015**, *119* (52), 15919−15928.

(30) The Diffusion Barrier Technique for Accurate and Reproducible Protein Mobility Measurement. https://www.malvernpanalytical.com/en/learn/knowledge-center/application-notes/an120906diffusionbarriertechnique (accessed November 20, 2023).

(31) Kaszuba, M.; Corbett, J.; Watson, F. M. N.; Jones, A. High-Concentration Zeta Potential Measurements Using Light-Scattering Techniques. *Philos. Trans. R. Soc. A: Math. Phys. Eng. Sci.* **2010**, *368*, 4439−4451.

(32) Waters Gradient Chromatograhy Calculator. https://www.waters.com/webassets/other/lp/prep_calc/AnalyticaltoPrep/NewPrepcalculator.htm (accessed November 20, 2023).

(33) Crawford, M. A.; Ward, A. E.; Gray, V.; Bailer, P.; Fisher, D. J.; Kubicka, E.; Cui, Z.; Luo, Q.; Gray, M. C.; Criss, A. K.; Lum, L. G.; Tamm, L. K.; Letteri, R. A.; Hughes, M. A. Disparate Regions of the Human Chemokine CXCL10 Exhibit Broad-Spectrum Antimicrobial Activity against Biodefense and Antibiotic-Resistant Bacterial Pathogens. *ACS Infect. Dis.* **2023**, *9* (1), 122−139.

(34) Roccatano, D.; Colombo, G.; Fioroni, M.; Mark, A. E. Mechanism by Which 2,2,2-Trifluoroethanol/Water Mixtures Stabilize Secondary-Structure Formation in Peptides: A Molecular

Dynamics Study. *Proc. Natl. Acad. Sci. U.S.A.* **2002**, *99* (19), 12179−12184.

(35) Tulumello, D. V.; Deber, C. M. SDS Micelles as a Membrane-Mimetic Environment for Transmembrane Segments. *Biochemistry* **2009**, *48* (51), 12096−12103.

(36) Crawford, M. A.; Fisher, D. J.; Leung, L. M.; Lomonaco, S.; Lascols, C.; Cannatelli, A.; Giani, T.; Rossolini, G. M.; Doi, Y.; Goodlett, D. R.; Allard, M. W.; Sharma, S. K.; Khan, E.; Ernst, R. K.; Hughes, M. A. CXC Chemokines Exhibit Bactericidal Activity against Multidrug-Resistant Gram-Negative Pathogens. *mBio* **2017**, *8* (6), No. e01549-17, DOI: 10.1128/mBio.01549-17.

(37) Crawford, M. A.; Timme, R.; Lomonaco, S.; Lascols, C.; Fisher, D. J.; Sharma, S. K.; Strain, E.; Allard, M. W.; Brown, E. W.; McFarland, M. A.; Croley, T.; Hammack, T. S.; Weigel, L. M.; Anderson, K.; Hodge, D. R.; Pillai, S. P.; Morse, S. A.; Khan, E.; Hughes, M. A. Genome Sequences of Multidrug-Resistant, Colistin-Susceptible and -Resistant Klebsiella Pneumoniae Clinical Isolates from Pakistan. *Genome Announc.* **2016**, *4* (6), No. e01419-16, DOI: 10.1128/genomeA.01419-16.

(38) Rampersad, S. N. Multiple Applications of Alamar Blue as an Indicator of Metabolic Function and Cellular Health in Cell Viability Bioassays. *Sensors* **2012**, *12* (9), 12347−12360.

(39) Crawford, M. A.; Zhu, Y.; Green, C. S.; Burdick, M. D.; Sanz, P.; Alem, F.; O'Brien, A. D.; Mehrad, B.; Strieter, R. M.; Hughes, M. A. Antimicrobial Effects of Interferon-Inducible CXC Chemokines against Bacillus Anthracis Spores and Bacilli. *Infect. Immun.* **2009**, *77* (4), 1664−1678.

(40) Crawford, M. A.; Burdick, M. D.; Glomski, I. J.; Boyer, A. E.; Barr, J. R.; Mehrad, B.; Strieter, R. M.; Hughes, M. A. Interferon-Inducible CXC Chemokines Directly Contribute to Host Defense against Inhalational Anthrax in a Murine Model of Infection. *PLoS Pathog.* **2010**, *6* (11), No. e1001199, DOI: 10.1371/journal.ppat.1001199.

(41) Crawford, M. A.; Lowe, D. E.; Fisher, D. J.; Stibitz, S.; Plaut, R. D.; Beaber, J. W.; Zemansky, J.; Mehrad, B.; Glomski, I. J.; Strieter, R. M.; Hughes, M. A. Identification of the Bacterial Protein FtsX as a Unique Target of Chemokine-Mediated Antimicrobial Activity against Bacillus Anthracis. *Proc. Natl. Acad. Sci. U.S.A.* **2011**, *108* (41), 17159−17164.

(42) Crawford, M. A.; Margulieux, K. R.; Singh, A.; Nakamoto, R. K.; Hughes, M. A. Mechanistic Insights and Therapeutic Opportunities of Antimicrobial Chemokines. *Semin. Cell Dev. Biol.* **2019**, *88*, 119−128.

(43) Luo, P.; Baldwin, R. L. Mechanism of Helix Induction by Trifluoroethanol: A Framework for Extrapolating the Helix-Forming Properties of Peptides from Trifluoroethanol/Water Mixtures Back to Water. *Biochemistry* **1997**, *36* (27), 8413−8421.

(44) Iatridi, Z.; Tsitsilianis, C. Water-Soluble Stimuli Responsive Star-Shaped Segmented Macromolecules. *Polymers* **2011**, *3* (4), 1911−1933.

(45) Zhang, Y.; Chen, M.; Luo, X.; Zhang, H.; Liu, C.; Li, H.; Li, X. Tuning Multiple Arms for Camptothecin and Folate Conjugations on Star-Shaped Copolymers to Enhance Glutathione-Mediated Intracellular Drug Delivery. *Polym. Chem.* **2015**, *6* (12), 2192−2203.

(46) Shiloh, M. U.; Ruan, J.; Nathan, C. Evaluation of Bacterial Survival and Phagocyte Function with a Fluorescence-Based Microplate Assay. *Infect. Immun.* **1997**, *65* (8), 3193−3198.

(47) Peptide Cutter. https://web.expasy.org/peptide_cutter/ (accessed November 20, 2023).

(48) Blum, A. P.; Kammeyer, J. K.; Yin, J.; Crystal, D. T.; Rush, A. M.; Gilson, M. K.; Gianneschi, N. C. Peptides Displayed as High Density Brush Polymers Resist Proteolysis and Retain Bioactivity. *J. Am. Chem. Soc.* **2014**, *136* (43), 15422−15437.